Environmental Science and Pollution Research (2021) 28:5755–5773
https://doi.org/10.1007/s11356-020-10728-w

RESEARCH ARTICLE

Functional and network analyses of human exposure to long-term evolution signal

Lei Yang[1] · Chen Zhang[1] · Zhiye Chen[2] · Congsheng Li[1] · Tongning Wu[1]

Received: 8 June 2020 / Accepted: 2 September 2020 / Published online: 25 September 2020
© Springer-Verlag GmbH Germany, part of Springer Nature 2020

Abstract

Human exposure to the electromagnetic field emitted by wireless communication systems has raised public concerns. There were claims of the potential association of some neurophysiological disorders with the exposure, but the mechanism is yet to be established. The wireless networks, recently, experience a transition from the 4th generation (4G) to 5th generation (5G), while 4G long-term evolution (LTE) is still the frequently used signal in wireless communication. In the study, exposure experiments were conducted using the LTE signal. The subjects were divided into sham and real exposure groups. Before and after the exposure experiments, they underwent functional magnetic resonance imaging. Within-session and between-session comparisons have been executed for functional connectivity and network properties. Individual specific absorption rate (SAR) was also calculated. The results indicated that acute LTE exposure beneath the safety limits modulated both the functional connection and graph-based properties. To characterize the effect of functional activity, SAR averaged over a certain tissue mass was not an appropriate metric. The potential neurophysiological effect of 5G exposure has also been discussed in the study.

Keyword Long-term evolution · Functional connectivity · Brain network · Specific absorption rate (SAR) · Electromagnetic hypersensitivity · Safety limits · Functional magnetic resonance imaging (fMRI)

Introduction

With the rapid advancement of wireless communication technology, radiofrequency (RF) electromagnetic field (EMF) exposure to potential health risks raised public concerns. To limit the RF-EMF exposure based on thermal effect, the safety guidelines (ICNIRP 2020; IEEE 2019) have been revised by the International Commission on Non-ionizing Radiation Protection (ICNIRP) and Institute of Electrical and Electronics Engineers (IEEE). These guidelines adopted the specific absorption rate (SAR) over a certain tissue mass as the metric for the frequencies below 6 GHz, the popular spectrum for current wireless communication technologies. Several behavioral and neurological effects claimed to be associated with EMF exposure, has been reported beneath the safety limits (Repacholi 1999). Moreover, some studies substantiated evidence for electromagnetic hypersensitivity (EHS), which includes visual (McCarty et al. 2011) and working memory disturbances (Zubko et al. 2017). Subsequently, the researchers have extensively explored the neurological effects from a variety of neurophysiological endpoints, e.g., cortical electrical activity (Hamblin et al. 2006; Croft et al. 2010; Lustenberger et al. 2013; Roggeveen et al. 2015a; Roggeveen et al. 2015b), cortical excitability (Tombini et al. 2013), cerebral blood flow (Aalto et al. 2006), brain glucose metabolism (Volkow et al. 2011), and hemodynamic responses (Volkow et al. 2011; Curcio et al. 2012). However, the outcomes were inconsistent, and the resultant effects were believed to be dependent on frequencies and modulations (Zhang et al. 2017).

In recent times, the wireless networks experience a transition from the 4th generation (4G) to 5th generation (5G). 4G long-term evolution (LTE) is still the widely used signal in wireless communication. The resting-state (RS) functional magnetic resonance imaging (fMRI) was applied to analyze the amplitude of spontaneous low-frequency function (ALFFs) and fractional ALFF (fALFF) (Lv et al. 2014) on regional segregation and data-driven functional connectivity

Responsible Editor: Lotfi Aleya

✉ Tongning Wu
wutongning@caict.ac.cn

[1] China Academy of Information and Communications Technology, Beijing, China

[2] Hainan Hospital of Chinese People's Liberation Army General Hospital, Beijing, China

(FC) (Wei et al. 2019). These results consistently validated the simultaneous modulation of different brain units owing to the LTE-EMF exposure. By LTE exposure, the decreased EEG alpha and beta band power (Yang et al. 2016) and the altered interhemispheric synchronization pattern of EEG activation (Lv et al. 2014a, b) have also been reported. Furthermore, the lack of effect on awake EEG has also been published (Nakatani-Enomoto et al. 2020).

As known, the human brain functions as an interconnected network that responds to external stimuli. The whole-brain functional and network analysis was expected to reveal comprehensive knowledge on the effect across different brain regions. Moreover, numerous studies suggested that the organization of the brain networks could be characterized by the graph theory-based approaches (Rubinov and Sporns 2010). In such a case, the network study would provide deeper insight into the acute effect of LTE-EMF exposure. The study also elucidated the applicability of the current dosimetric metrics for quantifying the neurophysiological effect. The possible reasons for the inconsistency were investigated. Extrapolation of the results to the EMF exposure of next-generation signals was discussed.

Method and Material

Subjects and the experimental procedures

The present study involved 34 right-handed subjects (19 males and 15 females, age between 19 and 36 years with the mean ± stdv as 23.6 ± 4.8 years old). The researchers selected the candidates with the history of neurological or psychiatric disorders by questionnaire. The participants were instructed to limit their phone usage for less than 10 min during the day prior to the experiments, and they reported using mobile phones against the ear for less than 1 h per day in the past 30 days.

In the double-blind experiment, the participants were equally divided into two groups for real and sham exposure, each comprising of 17 subjects (Table 1). During the experiment, the subject received one structural and one functional MRI before the exposure (real or sham blind to the subjects) and one fMRI after exposure. The duration of the exposure was 30 min for each session. During the exposure, participants were instructed to select a comfortable posture on the chair and to maintain the posture. Located in the MRI control room, the exposure room was shielded to prevent environmental EMF and noise. The subjects were asked to move slowly between the MRI bench and the exposure chair. The time interval between the exposure and the fMRI scan was 1 min. They were asked to report whether they fell asleep during the scan, and no monitoring system was applied in the experiment. The experimental scenario is illustrated in Fig. 1. The study was approved by the ethics committee of the People's Liberation Army General Hospital (Beijing, China). The participants signed consent after being explained the experimental procedure in detail.

Table 1 Demographic data for the subjects and the division of the experimental group

	Real exposure		Sham exposure	
	Male	Female	Male	Female
	9	8	10	7
Total	17		17	

Exposure system

The time-division LTE signal with a carrier frequency of 2.573 GHz was generated by a signal generator (CMW 500, R&S, Munich, Germany) and amplified by an RF power amplifier (AR40S1G4, AR, Bothell, WA), which were further delivered to a standard dipole (D2600V2, SPEAG, Zurich, Switzerland). The applied radio frame (total length: 10 ms) consisted of 2 half-frames of equal length. Each half-frame had 5 subframes, each 1 ms in length. In the exposure experiment, the maximal emission configuration was opted (6 uplink subframes in the radio frame). The radiation duration (including the uplink subframes and uplink pilot time slot subframes) accounted for 63.3% of the total frame length. Two power meters (E4416A, Keysight, Santa Clara, CA) were incorporated in the power input chain to achieve the constant output to the dipole regardless of the individual dielectric variation (Wu et al. 2012). The power was adjusted to 24 dBm (mean value). It is the theoretical maximal emission by an LTE terminal.

MRI Scan

A 3.0 T scanner (SIGNA EXCITE, GE Healthcare, Chicago, IL) with a conventional eight-channel phased array coil at PLA General Hospital (Beijing, China) was adopted in the study. The magnetic gradient field was 40 mT/m and the slew rate was 150 mT/m/s. The structural MRI scan was acquired with a three-dimensional fast spoiled gradient echo (3D FSPGR) sequence with the following parameters: repetition time (TR) = 6.8 ms, echo time (TE) = 2.9 ms, slice thickness = 1 mm, slice gap = 0 mm, field of view (FOV) = 22 cm × 22 cm, flip angle (FA) = 15°, matrix size = 256 × 256, in-plane resolution = 1.0 × 1.0 mm, number of excitations (NEX) = 1, and number of sagittal slices = 188. The functional images were obtained by an echo-planar imaging (EPI) sequence with the following parameters: TR = 2 s, TE = 30 ms, slice thickness = 3 mm, slice gap = 0.8 mm, FOV = 22 × 22 cm, FA = 90°, matrix size = 64 × 64, in-plane resolution = 3.4 × 3.4 mm,

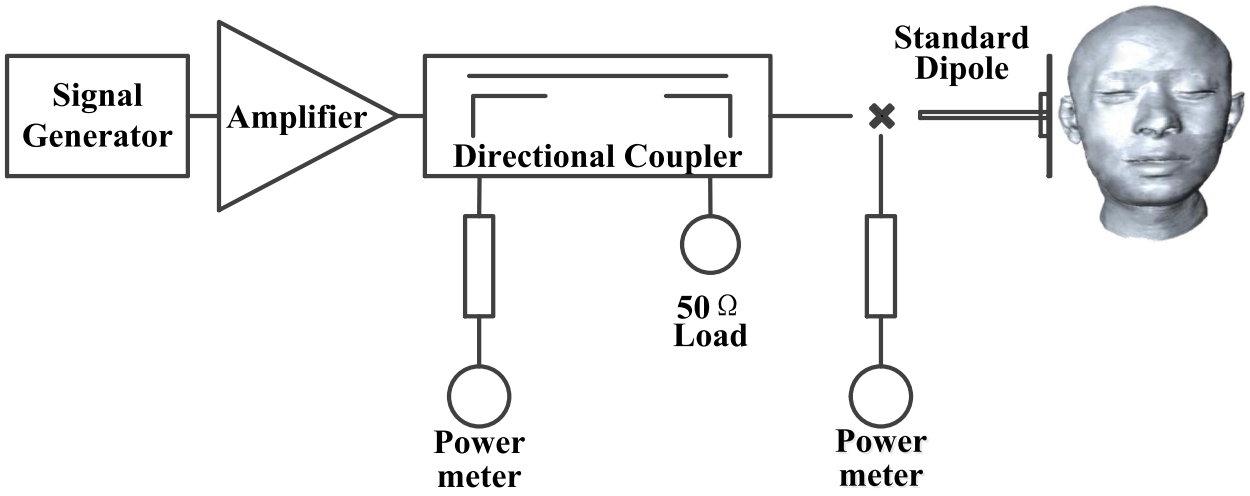

a

b c

Fig. 1 Exposure scenarios. **a** Power chain for exposure. **b** Instruments used in the experiments. **c** Subject under exposure

NEX = 1, and 32 transverse slices. The RS-fMRI scan acquired 180 image volumes and lasted for 6 min.

Data preprocessing

Firstly, the raw data (DICOM format) from the MRI scanner was transformed to NIfTI format. The first 10 volumes of the images were discarded for magnetization equilibrium. Consequently, slice timing correction and head motion correction were conducted for the remaining 170 volumes. No dataset was excluded from the analysis due to the excessive head movement (the threshold was defined as translation > 2 mm or rotation > 2°). The individual T1-weighted images were co-registered to the mean functional image after motion correction, thereafter classified into gray matter (GM), white matter (WM), and cerebrospinal fluid (CSF). The resulting GM and WM images were nonlinearly registered into MNI space, and the transferring parameters were estimated. All the functional images were then normalized into this space with the help of these parameters, and the normalized images were further smoothed using a [6 mm × 6 mm × 6 mm] full width at half maximum Gaussian kernel. Detrend was performed to reduce the linear and non-linear drift in the signal. A band-pass filter was applied to filter the time series of each voxel (0.01–0.1 Hz). The nuisance signals (global signal, CSF, and WM signals) were regressed out from each voxel's time course. The processed images could be used for network analysis. The data preprocessing pipeline was conducted using SPM8 (Penny et al. 2011) and DPARSF (Yan and Zang 2010).

FC metrics

To define the nodes and edges for network analysis, the preprocessed data were parceled to certain brain atlas, e.g., Anatomical Automatic Labeling (AAL) atlas (Tzourio-Mazoyera et al. 2002). Consequently, time-course data were averaged from each parceled brain unit for computing the

pair-wise correlation coefficients. As a result, an N × N correlation matrix (N is 90, representing the number of parceled brain regions) was generated. Fisher's Z transformation was performed to improve the normality of the correlation. Only the positive correlations were taken into consideration in this study because the negative ones were believed to degrade the reliability of the result (Wang et al. 2011). Connectivity strength and its diversity were consequently conducted for the regional properties of the FC matrices.

FC strength

The metric denoted the average value of the correlations between the ith node and all other nodes of the brain as described by Eq.(1):

$$\overline{R}(i) = \frac{\sum_j r_{i,j}}{N-1} \tag{1}$$

where $r_{i,j}$ is the correlation coefficient for nodes i and j.

Diversity of connections

The regional diversity of connections was the variance of the correlations between the ith node and all other nodes as given by Eq.(2):

$$\mathrm{Var(R(i))} = \frac{\sum_j \left(r_{i,j} - \overline{R}(i)\right)^2}{\mathrm{N}-1} \tag{2}$$

The global FC values can be obtained by averaging the nodal connectivity strength and their diversity across all the nodes.

Brain network metrics

To explore the topological characteristics of the network, thresholding based on connection sparsity was applied, i.e., the ratio of the number of actual edges divided by the maximum possible number of edges in the network. The threshold values were set such that all the nodes in the investigated graphs were connected to at least one other node (the graphs were not fragmented), and the graph had nonrandom properties (densely connected graphs presented non-biological features according to Kaiser and Hilgetag (2006)). As such, connection sparsity was derived with a range of 35–50%. The results of the brain network were averaged over this range, with a 1% increment (Bassett et al. 2008). The following metrics were assessed in the study.

Degree $k(i)$ is equal to the number of edges connecting the ith region to the rest of the network:

$$k(i) = \sum_j A_{i,j} \tag{3}$$

where A is the binary adjacency matrix obtained by thresholding the functional connectivity matrix.

Regional efficiency $E(i)$ is computed for each node in a graph,G, as follows:

$$E(i) = \frac{1}{N-1} \sum_{j \in G} \frac{1}{L_{i,j}} \tag{4}$$

where $L_{i,j}$ is the minimum path length between regions i and j. The global efficiency is the mean value over all the regional results.

The clustering coefficient $C(i)$ of a node v is the ratio of connected triangles, δ_v, to connected triples, τ_v. The clustering coefficient of a graph is as follows:

$$C(G) = \frac{1}{|V'|} \sum_{v \in V'} \frac{\delta_v}{\tau_v} \tag{5}$$

where V' is the set of nodes with degree > 2.

Clustering coefficient (C) is a measure of grouping within the network, indicating how likely the neighbors of a node are to be connected with one another. Path length, L, can be estimated as the inversed efficiency.

Small-worldness is represented as the normalized clustering coefficient divided by the normalized path length. The normalized clustering coefficient and characteristic path length are the division of clustering coefficient C and characteristic path length L to the clustering and path length of a comparable random graph (Watts and Strogatz 1998).

Assortativity is a measure of the correlation between the degree of a node and the mean degree of its nearest neighbors. A positive value of degree correlation signifies that nodes are likely to be connected to other nodes with the same degree and, therefore, that the high degree nodes or hubs of the network are likely to be connected to each other. If the degree correlation is negative, this implies that the hubs of the network are not connected to each other, which is a characteristic of a disassortative network.

Hierarchy (β) of the networks is a parameter of the power-law relationship between clustering C and degree k of the nodes in the network: $C \sim k^{-\beta}$. β can be calculated by fitting a linear regression line to the plot of $\log(C)$ versus $\log(k)$ for the network. A large positive value of β signifies the hubs of the network have a high degree (total connectivity) but low clustering (local connectivity), indicating that they are connected predominantly to nodes not otherwise connected to each other.

Synchronization measures the propensity that all nodes fluctuate in the same wave pattern. The detailed formula could be referred to in the literature (Rubinov and Sporns 2010).

The abovementioned functional and network parameters were computed using MATLAB based toolkit Gretna (Wang et al. 2015).

Network comparison

The statistical comparison was computed for the functional and network metrics. The paired t-test was conducted for the within-session comparison, and the independent sample t-test was applied for the between-session comparison. For both cases, the false discovery rate (FDR) was used for multiple corrections. A value of $p < 0.05$ was considered as the threshold for statistical significance. The data analysts were blind to the source of the data.

Individual SAR calculation

The anatomical head model was automatically reconstructed from the preprocessed individual structural images following the procedures by Li et al. (2015) using an in-house segmentation tool (Wu et al. 2013; Li and Wu 2015) and iSeg (Zurich Med Tech AG). The generated head models contained 10 tissues at the resolution of 1 mm^3. Consequently, Finite-Difference Time-Domain (FDTD) simulation was performed to ascertain the power absorption in the experiment per subject. Peak SAR averaged over 10 g tissue (pSAR10g) and over 1 g tissue (pSAR1g) was presented for each subject.

Correlation between variables

We explored associations between the functional parameters, graph-based metrics, and the individual peak SAR values using Pearson's correlation. The individual network difference (post-exposure value minus pre-exposure value) from the within-session real-exposure experiments and individual peak SAR were used for the study. The correlation coefficients elucidated the association between each pair of variables over all subjects in the study.

Results

Functional connection

FC maps averaged across all participants in the two groups are presented in Fig. 2. The global measures of FC strength and diversity of FC strength averaged over the two groups are detailed in Table 2.

Between-session comparison

Concerning the between-session results from the subjects after exposure, an insignificant difference in the between-session outcome in terms of global measures was detected for the subjects following exposure ($p > 0.1$). The nodal connectivity strength and diversity of connectivity strength are illustrated in Fig. 3. These two figures compared the difference in the post-exposure results. A prominent increase in FC strength was witnessed at contralateral middle frontal gyrus (MFG_L) and insula (INS_L), bilateral triangular part of inferior frontal gyrus (IFGtriang_L and IFGtriang_R) and Heschl gyrus (HES_L and HES_R), and contralateral lenticular nucleus putamen (PUT_R). On the contrary, a significant reduction of diversity of FC strength was evident at contralateral parahippocampal gyrus (PHG_R) and ipsilateral posterior cingulate gyrus (PCG_L).

No between-session difference was detected from the subjects prior to exposure.

Within-session results

The nodal within-session difference was identified in the real-exposure session. The changed regions were the same as those found in the between-session comparison and, therefore, the results were not repeated. The within-session results from the sham exposure group revealed a decrease at PUT_L, PUT_R, and increase at left and right posterior cingulate gyrus (PCG_L, PCG_R), PUT_R and INS_R, INS_L in terms of FC strength ($p < 0.01$). The diversity of FC strength diminished at PUT_L and PUT_R, whereas enhanced at INS_R and PCG_R ($p < 0.015$). The results are described in Fig. 4.

Brain network results

Global metrics: efficiency, assortativity, hierarchy, small-worldness, and synchronization.

Between-session comparison The global metrics were compared and are depicted in Table 3. Figure 5 highlights the mean results of the global metrics over the subjects from the two groups. Briefly, no significant between-group difference was observed in terms of Efficiency, Assortativity, and Hierarchy. However, synchronization of the network was reduced by the real exposure group ($p = 0.018$, $t = -2.495$). The small-worldness was significantly raised by EMF exposure ($p = 0.004$, $t = 3.071$), which could be attributed to the increased normalized clustering coefficient ($p = 0.033$, $t = 2.227$).

There was no difference between the before-exposure results.

Within-session comparison The results from the sham-exposure session failed to portray any significant difference. In contrast, we perceived significant differences from the real-exposure session. Small-worldness enhanced owing to EMF exposure ($p = 0.019$, $t = 2.475$). The synchronization was marginally decreased by real exposure ($p = 0.042$, $t = -2.115$). There was increase in the normalized clustering

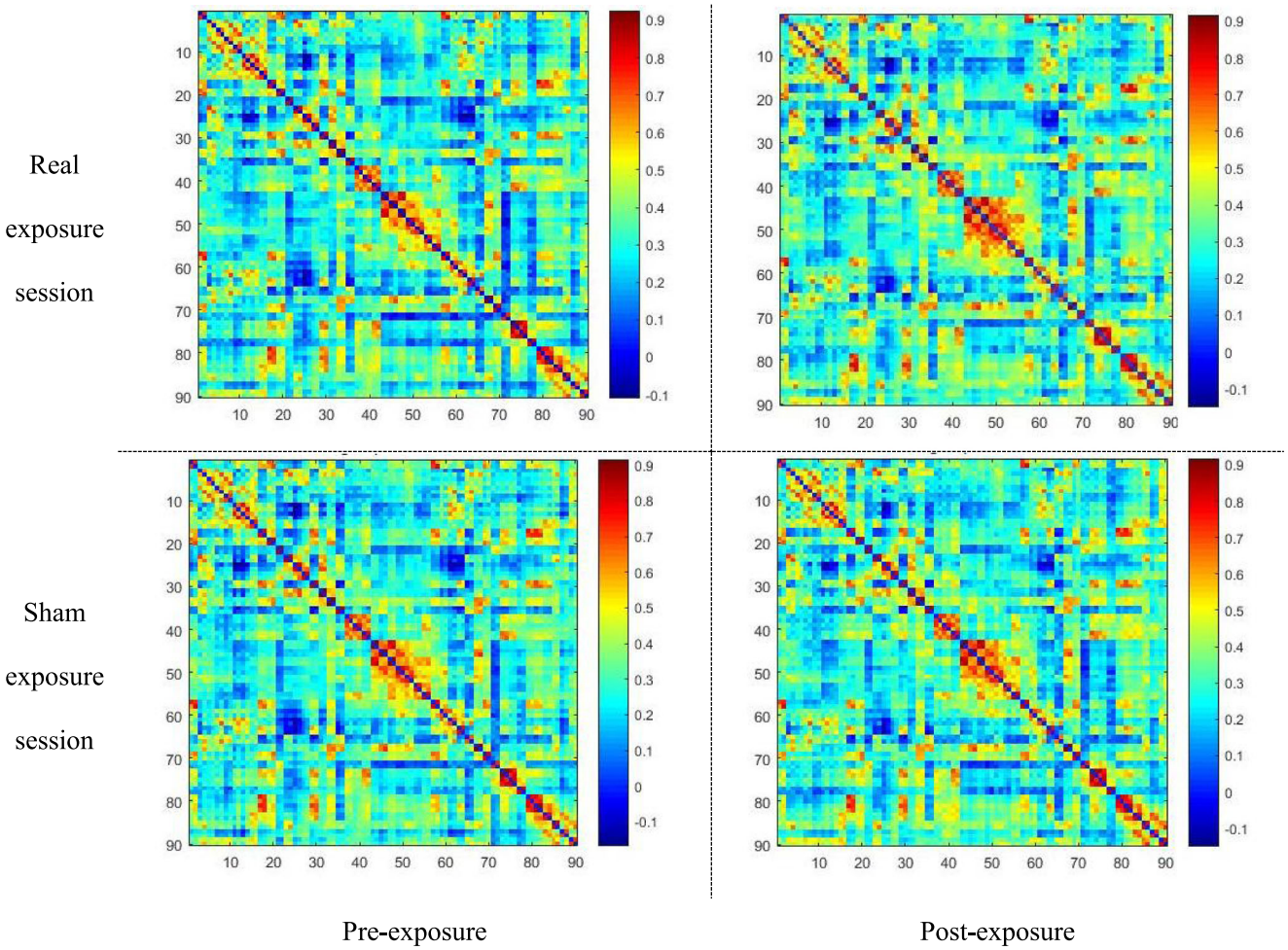

Fig. 2 FC matrices

coefficient ($p = 0.020$, $t = 2.456$). These changes were in accordance with those of the between-session comparison for the post-exposure results.

Nodal metrics: efficiency, degree centrality, and betweenness centrality.

The significant nodal changes by EMF exposure were summarized in Table 4.

Table 2 Global measures of FC metrics

Real exposure		
	Pre-exposure (mean ± stdv)	Post-exposure (mean ± stdv)
FC strength	0.334 ± 0.056	0.291 ± 0.050
FC diversity	0.048 ± 0.007	0.052 ± 0.009
Sham exposure		
	Pre-exposure (mean ± stdv)	Post-exposure (mean ± stdv)
FC strength	0.32 ± 0.051	0.304 ± 0.053
FC diversity	0.01 ± 0.008	0.049 ± 0.008

stdv: standard deviation

Between-session comparison The clustering coefficient was significantly increased at the bilateral frontal cortex (left supplementary motor area: SMA_L, left median cingulate and paracingulate gyri: DCG_L, IFGtriang_R, and DCG_R). The shortest path length was significantly enhanced at both sides of Calcarine fissure and the surrounding cortex (CAL_L and CAL_R). Accordingly, the nodal efficiency was significantly reduced at bilateral CAL. Figure 6 a illuminates the affected sites.

Within-session results The within-session results from the real-exposure session were comparable to those obtained from the between-session results. Briefly, EMF exposure significantly raised the clustering coefficient at left superior frontal gyrus, medial (SFGmed_L, close to SMA_L), DCG_L, DCG_R, and right inferior frontal gyrus, opercular part (IFGoper_R, adjacent to IFGtriang). A significant increase was also evident in the shortest path length at CAL_L and CAL_R, whereas the decrease was pronounced at HES_R. Consequently, the nodal efficiency was significantly enhanced at HES_R. Figure 6 b shows the affected sites.

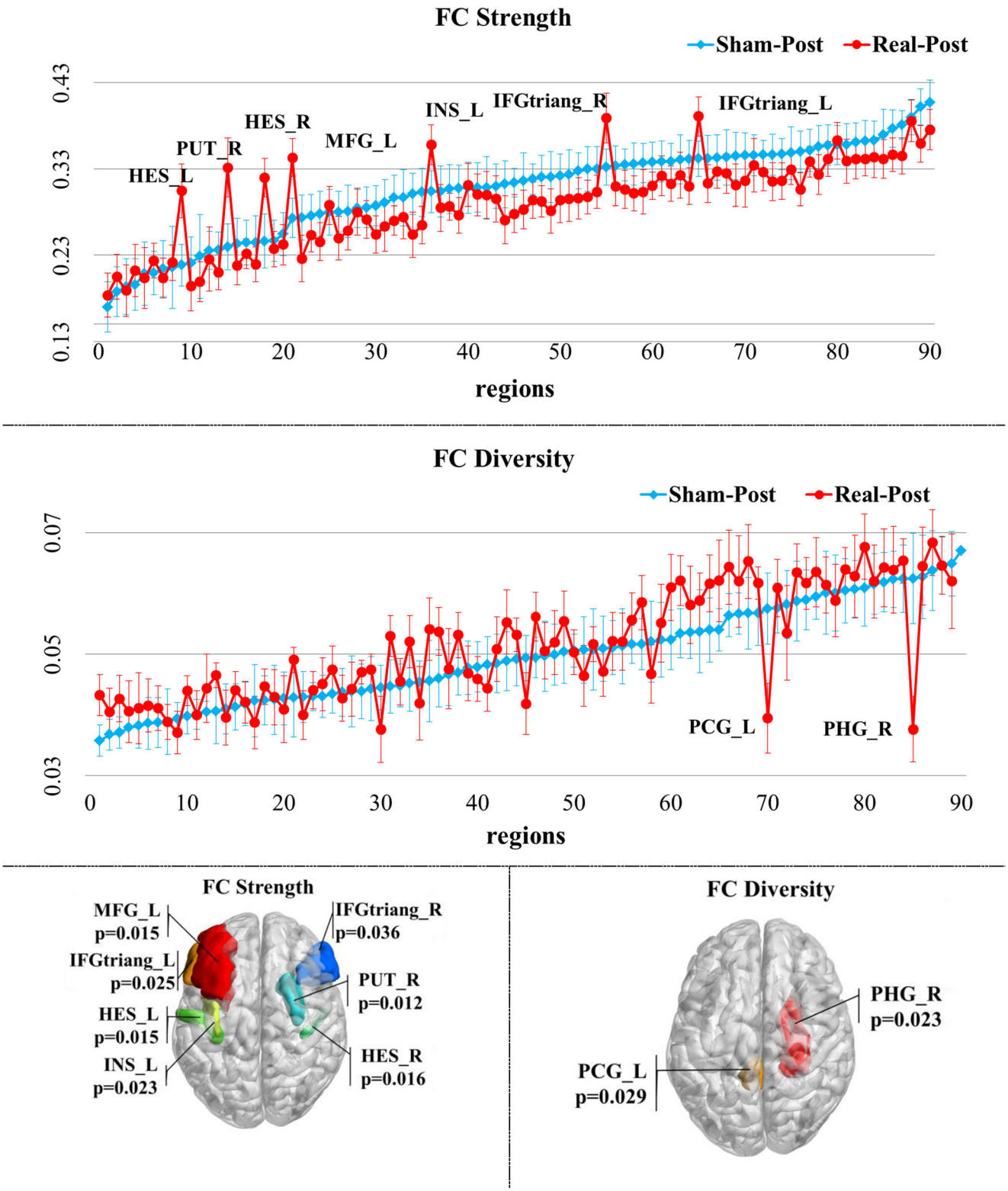

Fig. 3 Between-session post-exposure results of FC strength and diversity of FC strength. Sham-Post: post-exposure results from the sham session; Real-Post: post-exposure results from the real exposure session

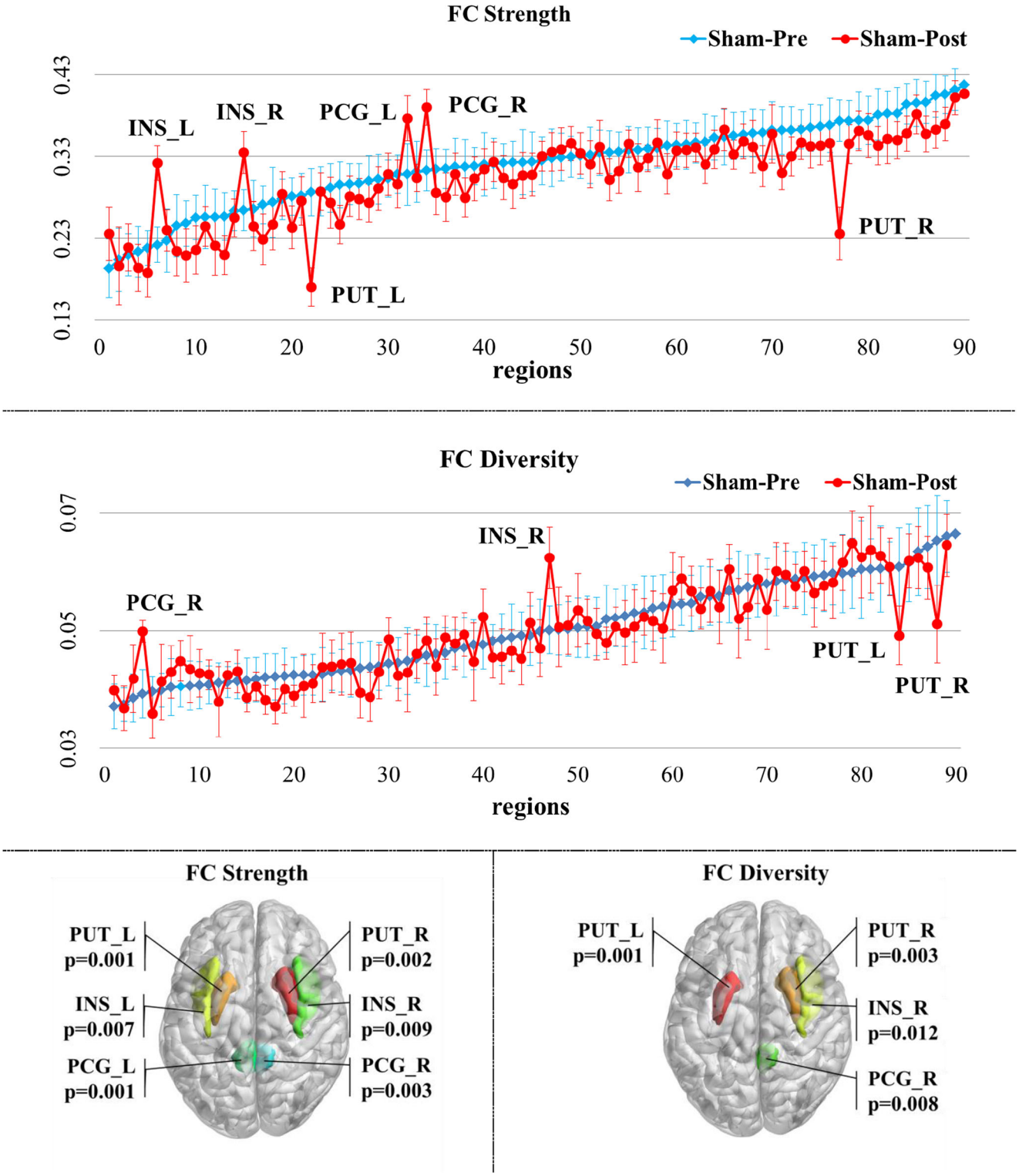

Fig. 4 Within-session results from the sham exposure group of FC strength and diversity of FC strength. Sham-Pre: pre-exposure results from the sham session; Sham-Post: post-exposure results from the sham session

The sham-exposure session introduced a significant reduction of the clustering coefficient for HES at double sides and enhancement of the hippocampus at the right side (HIP_R).

Power distribution in the head

The calculated peak SARs averaged over 10 g and 1 g tissues were obtained for each subject. The pSAR10g was 0.61 ± 0.14

Table 3 Network metrics averaged over subjects

	Real exposure session		Sham exposure session		Statistical comparison			
	Pre-exposure (mean ± stdv)	Post-exposure (mean ± stdv)	Pre-exposure (mean ± stdv)	Post-exposure (mean ± stdv)	t1	t2	t3	t4
Assortativity	0.163 ± 0.081	0.159 ± 0.063	0.16 ± 0.07	0.162 ± 0.076	0.903	0.911	0.943	0.872
Hierarchy	0.057 ± 0.101	0.082 ± 0.099	0.074 ± 0.095	0.064 ± 0.106	0.619	0.602	0.763	0.473
Network efficiency-global	0.699 ± 0.013	0.705 ± 0.006	0.702 ± 0.014	0.703 ± 0.006	0.261	0.613	0.904	0.157
Synchronization	0.109 ± 0.054	0.067 ± 0.062	0.114 ± 0.06	0.120 ± 0.063	0.018	0.710	0.364	0.042
Small world-normalized clustering	1.208 ± 0.060	01.270 ± 0.085	1.196 ± 0.066	1.203 ± 0.092	0.033	0.569	0.805	0.02
Small world-normalized path length	1.016 ± 0.0017	1.010 ± 0.007	1.013 ± 0.017	1.013 ± 0.008	0.669	0.352	0.214	0.889
Small worldness	1.19 ± 0.071	1.257 ± 0.088	1.17 ± 0.076	1.160 ± 0.096	0.004	0.439	0.744	0.019

t1: post-exposure results from the real session vs. post-exposure result from the sham session; t2: pre-exposure results from the real session vs. pre-exposure results from the sham session; t3: post-exposure results from the sham session vs. pre-exposure results from the sham session; t4: post-exposure results from the real session vs. pre-exposure results from the real session

W/kg, with a maximal value of 1.02 W/kg, while pSAR1g was 2.47 ± 0.65 W/kg, with a maximal value of 4.08 W/kg. The spatial SAR distribution is demonstrated in Fig. 7 for each subject.

Correlation of the network properties and the dosimetric results

The correlation matrix is shown in Fig. 8. A significant correlation was revealed in various functional and network metrics. It was justified because the network parameters were derived from the functional connections by thresholding. In contrast, none of these metrics correlated with pSAR1g nor with pSAR10g.

Discussion

Dose-effect relation

Figure 8 substantiated the positive or negative correlation between the functional and network properties, which was vindicated owing to the fact that the network properties were derived from the functional connections by thresholding. The analysis indicated that the individual SAR averaged over different tissue mass did not correlate with the functional connectivity strength, nor with the network properties. The results established that pSAR10g and pSAR1g were inappropriate to determine the neurological changes by EMF exposure. This could be explained by the fact that SAR limits were based on the power absorption in 10 g and 1 g tissue, thereby increasing the local temperature by an order of 0.1 °C (considering the safety factor). In contrast, the firing of a neuron could ensue by the temperature change of even less magnitude (Burek et al. 2019). The firing of one neuron may initiate the cascades or "avalanches" in the neuronal system, whereby activity propagates as individual neurons trigger action potential firing in subsequent neural networks (Beggs and Plenz 2003). The metrics based on macroscopic temperature rise over a certain tissue mass (comparable to the weight of millions of neurons) were incongruous to quantify the functional/network change triggered by a certain neuron. This could justify the inconsistency reported by the available literature.

Experiments with exposure at different levels are essential to validate this hypothesis. However, the ethics committee did not authorize the experimental protocol because it involved repetitive exposures for the subjects. Furthermore, exposure at different durations may also provide more insight into the results. Unfortunately, the same reason prohibited us from doing that.

Modulation of functional and network properties by LTE EMF exposure

Another novelty of the study was contributed by the whole-brain modulation in terms of functional connectivity and network topological properties by LTE exposure.

By exposure, functional connection strength was diminished, whereas its diversity enhanced slightly for most of the 90 regions (Fig. 3). However, an insignificant difference was established for these two global metrics (Table 2). From Table 3, it was evident that exposure increased the normalized clustering coefficient, while normalized characteristic path length remained unchanged. These two changes contributed to the significant increase in small worldness. The small-world architecture confirms the coexistence of segregation and integration of the brain network, which was believed to allow high rates of information processing and learning (Simard et al.

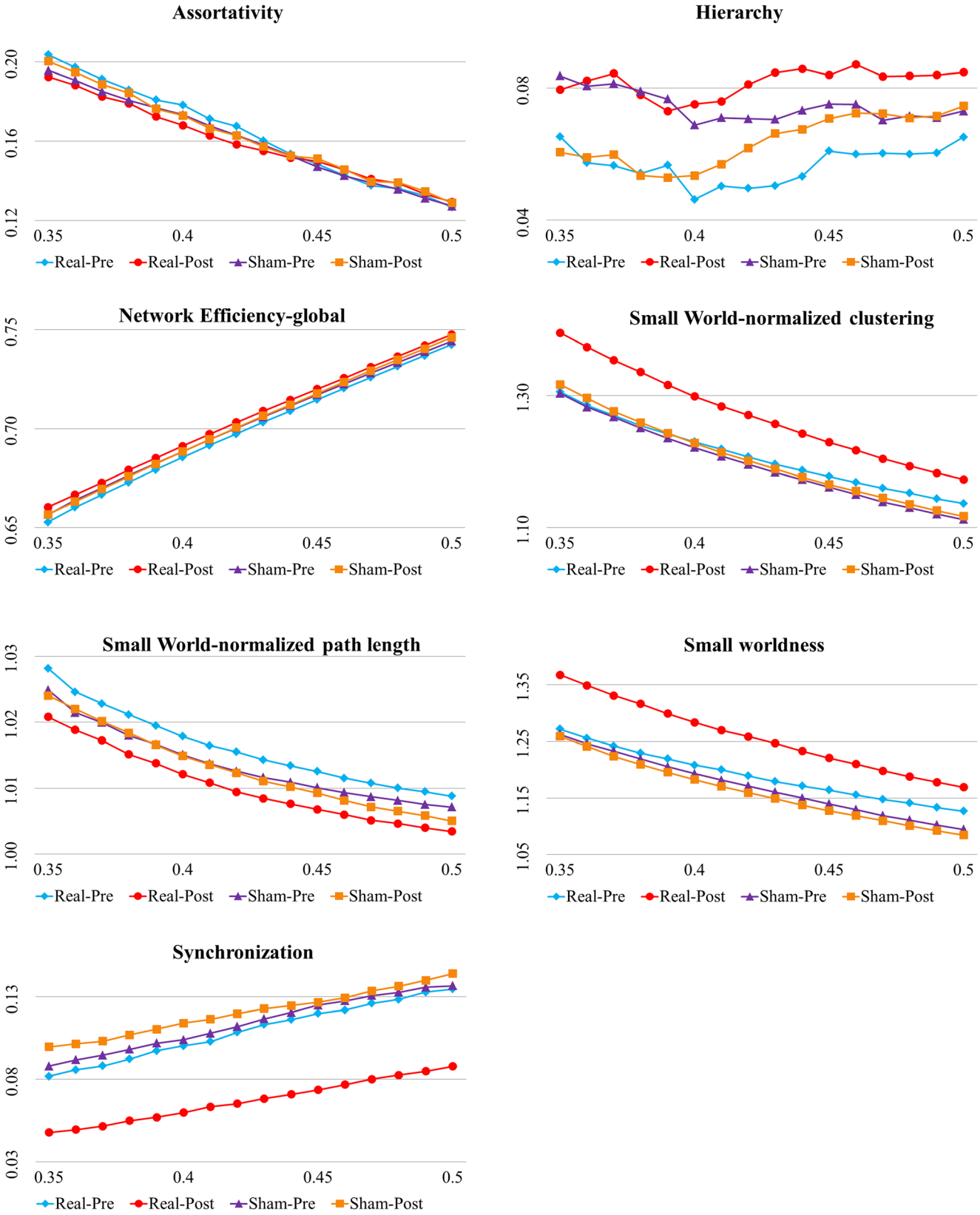

Fig. 5 Global network metrics. The results are presented for various sparsity thresholding values. real-pre: prior-exposure results from the real exposure group; real-post: post-exposure results from the real exposure group; sham-pre: prior-exposure results from the sham exposure group; sham-post: post-exposure results from the sham exposure group. The horizontal axis of this chart is thresholding value (sparsity)

Table 4 Significantly changed nodal metrics

	Clustering coefficient	Shortest path length	Nodal efficiency
t1	IFGtriang_R: p = 0.007, t = 2.905	CAL_L: p = 0.016, t = 2.566	*CAL_L*: p = 0.019, t = − 2.470
	SMA_L: p = 0.042, t = 2.123	CAL_R: p = 0.015, t = 2.581	*CAL_R*: p = 0.017, t = − 2.523
	DCG_R: p = 0.016, t = 2.550	/	/
	DCG_L: p = 0.010, t = 2.736		
t2	/	/	/
t3	*HES_R*: p = 0.042, t = − 2.120	/	/
	HES_L: p = 0.035, t = − 2.212		
	HIP_R: p = 0.032, t = 2.243		
t4	SFGmed_L: p = 0.036, t = 2.184	/	/
	DCG_L: p = 0.047, t = 2.058	CAL_L: p = 0.032, t = 2.232	*CAL_L*: p = 0.042, t = − 2.122
	DCG_R: p = 0.024, t = 2.264	CAL_R: p = 0.021, t = 2.423	*CAL_R*: p = 0.022, t = − 2.413
	IFGoperc_R: p = 0.006, t = 2.969	*HES_R:* p = 0.023, t = − 2.392	HES_R: p = 0.022, t = 2.401

t1: post-exposure results from the real session vs. post-exposure result from the sham session; t2: pre-exposure results from the real session vs. pre-exposure results from the sham session; t3: post-exposure results from the sham session vs. pre-exposure results from the sham session; t4: post-exposure results from the real session vs. pre-exposure results from the real session

2005). A higher level of small worldness, on the one hand, may facilitate information processing, but it could also indicate hyper-connectivity, unnecessarily beneficial to normal information processing. For example, elevated small-worldness has been documented for veterans with traumatic brain injury (TBI) and posttraumatic stress disorder (PTSD) in comparison to the veterans with TBI but without PTSD (Rowland et al. 2018). In particular, PTSD had syndromes as avoidance, arousal, perturbed moods, analogous to those claimed with EHS. Both between-session and within-session results revealed the reduction of network synchronization by EMF exposure. The metric explained the susceptibility of the network to the external stimulation (Hövel et al. 2018). It may indicate the disruption of the normal synchronization ability by LTE EMF exposure. A similar effect has also been reported by our EEG studies (Lv et al. 2014a, b) but not in a recent study (Nakatani-Enomoto et al. 2020).

A marked increase in the clustering coefficient was observed at the contralateral medial frontal lobe (SMA_L and MCG_L) and ipsilateral inferior and medial frontal lobe (IFGtriang_R, MCG_R). These regions are the locations involved in reward-based decision making, motor control, language processing, and speech production. (Price 2012). Enhanced efficiency following LTE EMF exposure was also witnessed for HES on both sides. Heschl gyrus is the location of the human primary auditory cortex, and its structural asymmetry may affect the way people process and perceive sensory information (Catherine et al. 2009). Calcarine fissure and surrounding cortex (CAL_L and CAL_R), considered to be the primary visual cortex (Engel et al. 1997), exhibited significantly reduced efficiency. The nodal clustering coefficient and nodal efficiency (shortest path length) quantified the capability for information transfer. With higher nodal efficiency, the information transfer consumed less energy. The results highlighted the suppression of the information exchange ability at the primary visual cortex but increased or unaffected ability at the other hubs in the dorsal visual pathway, possibly implying a perturbed visual information processing stream. The bilateral fronto-temporal cortical activation (MFG_L, IFGtriang_L, IFGtriang_R, HES_L, and HES_R) in terms of FC strength was prominent and in agreement with a large portion of the available human exposure studies (Zhang et al. 2017). The effect might indicate the enhanced cortical neural efficiency and simple cognitive-motor processes resulting from exposure to time-division signals (Vecchio et al. 2012). A significant reduction was also noted at PCG and INS. The insular cortex (insula and insular lobe) is involved in consciousness and plays a role in regulating emotion and the body's homeostasis (Menon and Uddin 2010). Situated in the cortical region in the medial temporal lobe that surrounds the hippocampus, the parahippocampal gyrus (PHG) is engaged in both spatial memory (Squire and Zola-Morgan 1991) and navigation (Aguirre et al. 1996; Maguire et al. 1996). Most of the sites are believed to play an important role in sensory, degenerative neurological disorders, and psychopathology. Alterations in these sites may have a potential association with a series of self-claimed symptoms (redness, tingling, and burning sensations) as well as neurasthenic and vegetative symptoms (fatigue, tiredness, concentration difficulties, dizziness, nausea, heart palpitation, and digestive disturbances), predicted to be due to EMF exposure. In our previous human studies, the brain changes in terms of fALFF and ReHo were explored. ALFF estimates the strength of regional neural activity (Zang et al. 2007), while the intraregional neural synchrony is characterized by ReHo (Zang et al. 2004). The functional and network metrics in the present study

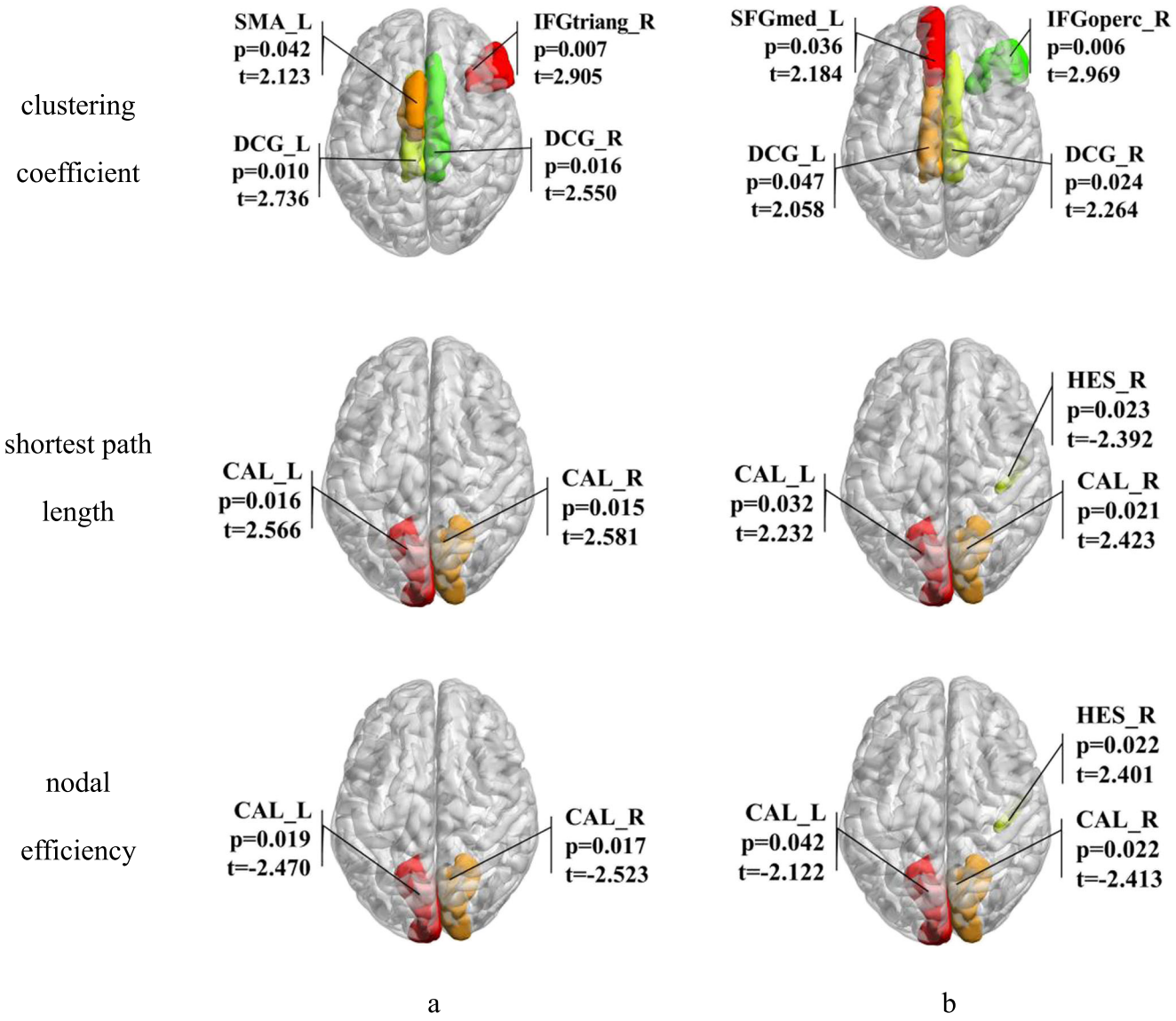

Fig. 6 Nodal changes. Significant changed sites by between-session comparison of the post-exposure results (**a**), and significant changed sites by with-session comparison from the sham-exposure group (**b**)

elucidate the intrinsic brain organization topology. With varied neurophysiological interpretations, these metrics should be integrated to provide a comprehensive view of the modulation of the brain by LTE exposure. In general, the modulated sites were consistent with these studies.

Some studies of other imaging modalities have also illuminated similar brain modulation. A PET study (Aalto et al. 2006) revealed that a mobile phone in operation triggered a local decrease in the regional cerebral blood flow beneath the antenna in the inferior temporal cortex and an increase in the prefrontal cortex. Volkow et al. (2011) used PET to evaluate brain glucose metabolism in humans for over 50 min during CDMA exposure. Increased metabolism was detected in the ipsilateral orbitofrontal cortex and temporal pole (side close to the antenna) during acute EMF exposure. Impact on frontotemporal regions was also evident from some ERD and ERP experiments (Vecchio et al. 2012; Vecchio et al. 2012; Vecchio et al. 2007).

During 3 T MRI scan, the subjects were exposed to the static magnetic field, gradient magnetic field, and the RF fields (128 MHz). The effect may confound the results and should be clarified. Previous reports proposed activation of the sites at the anterior cingulate, the insula, hippocampus, and some parts of nasal gandlia (caudate) following exposure to MRI (Robertson et al. 2009). Our study uncovered the alterations in insula, parahippocampal gyrus, hippocampus, and putamen, and they could be attributed to the effect of MRI exposure. To eliminate activation by the battery noise, the standard dipole was employed for exposure sources (Haarala et al. 2003). However, there was a loud sound during the scan. Although subjects were recommended to wear plastic earplugs, the exposure to sonic stimuli may, at least

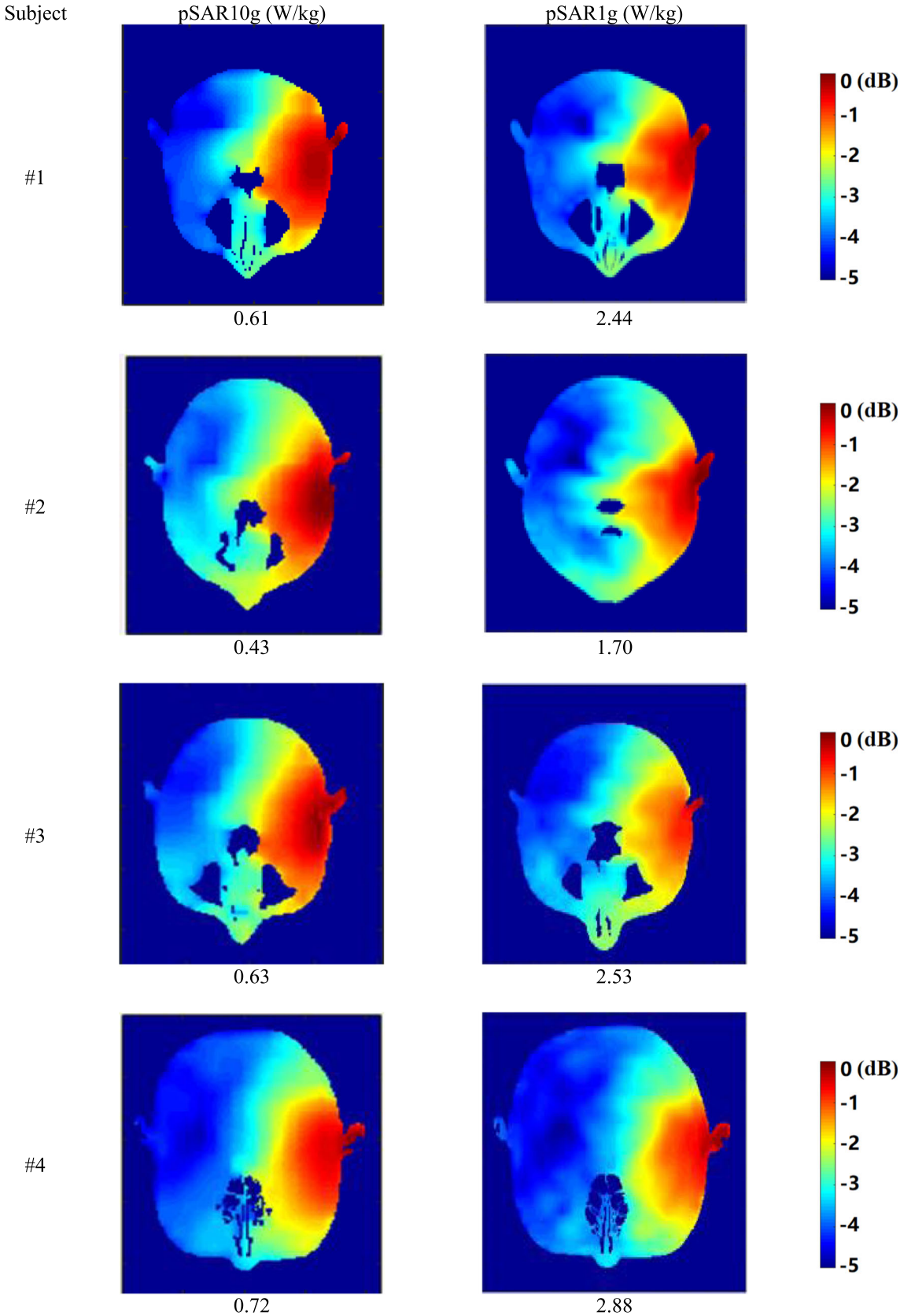

Fig. 7 SAR distribution of the subjects in the real-exposure group. The horizontal slices on the peak value level are selected

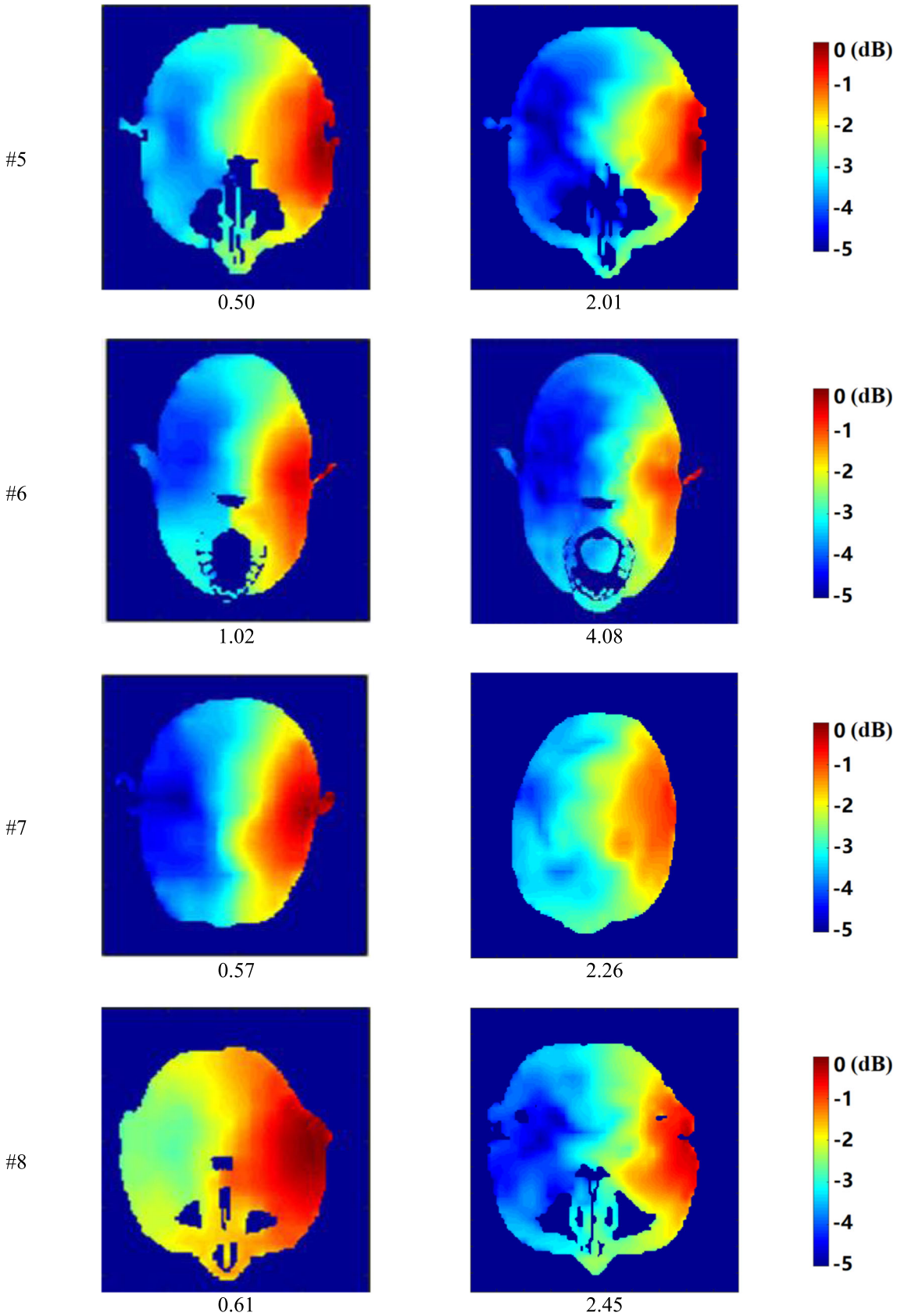

Fig. 7 (continued)

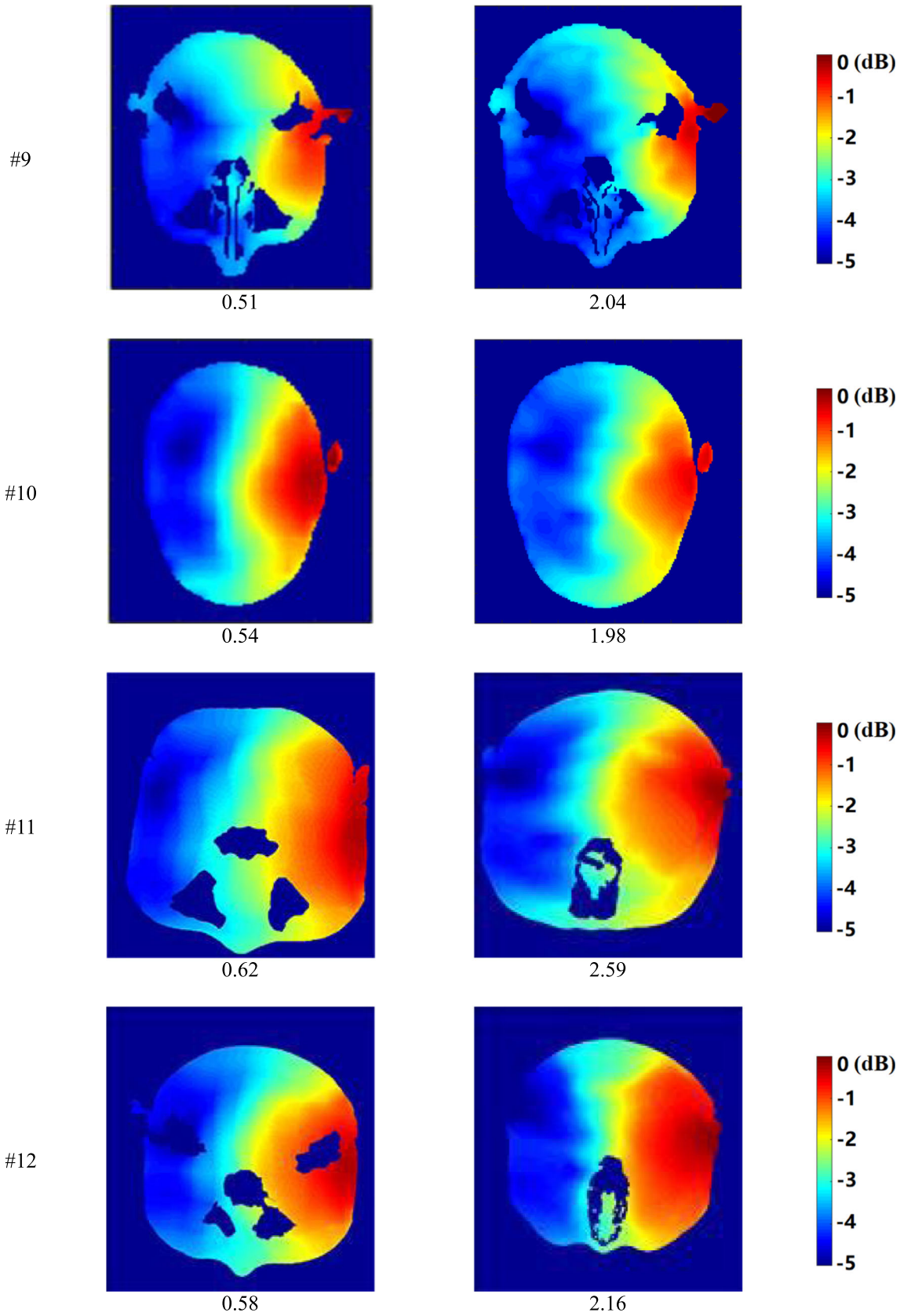

Fig. 7 (continued)

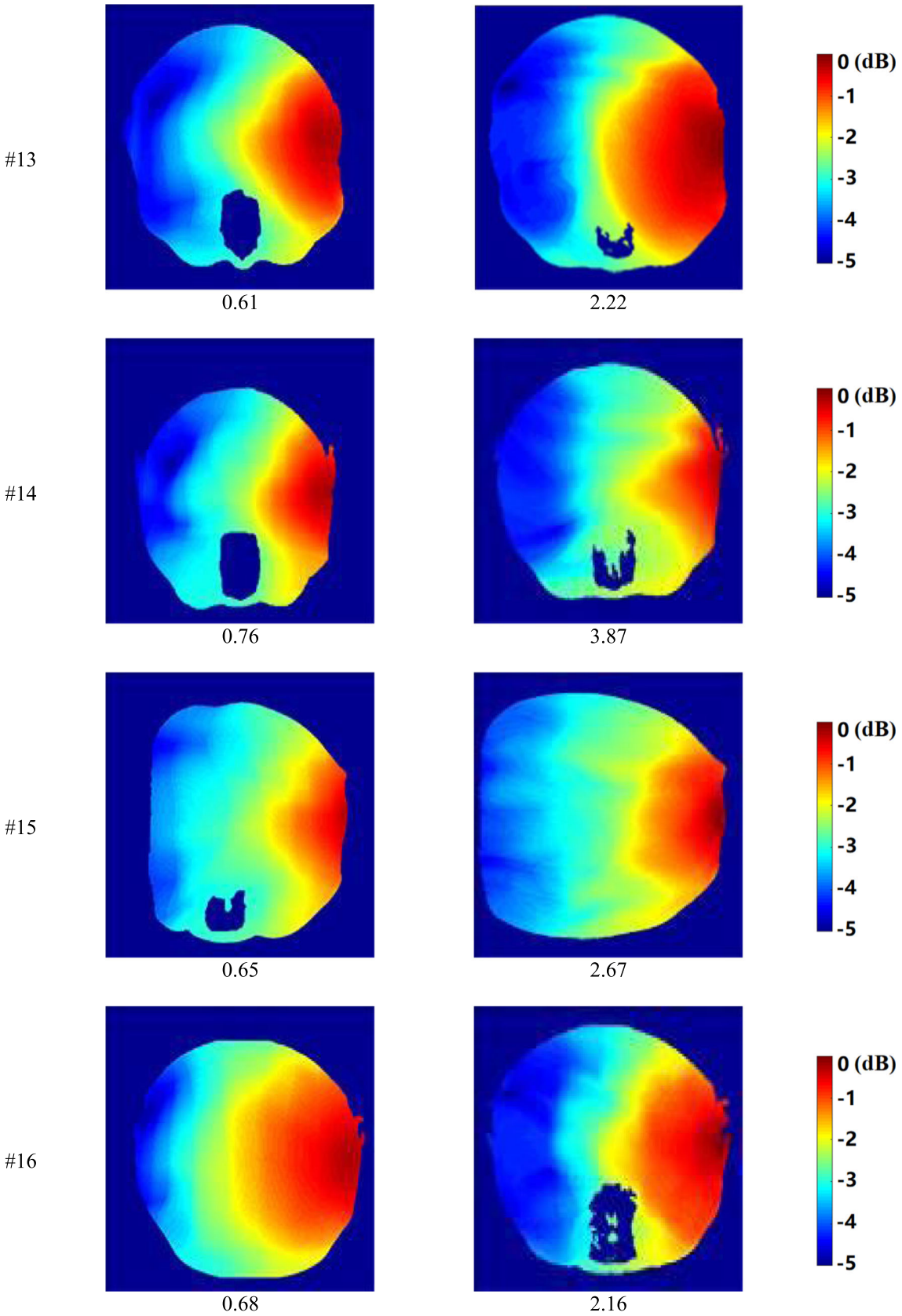

Fig. 7 (continued)

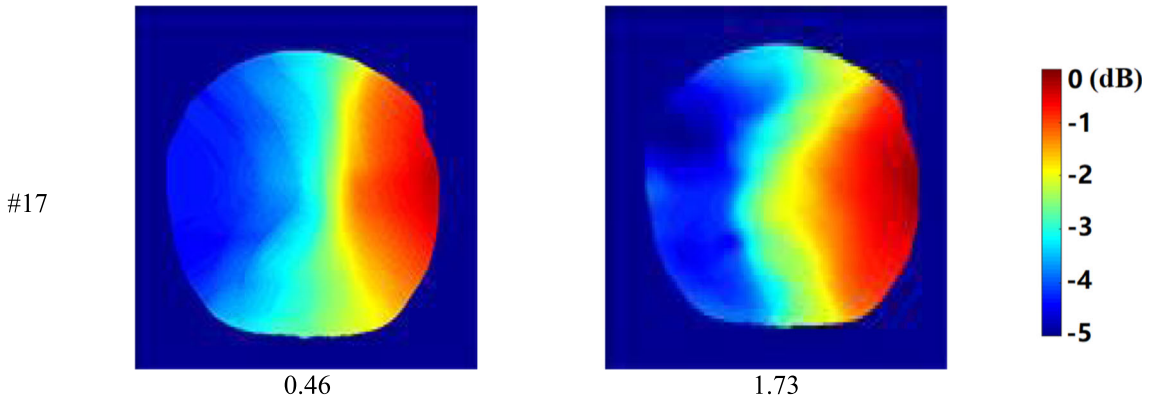

Fig. 7 (continued)

partially, contribute to the activation of auditory regions. The impact of these stimuli needs to be elucidated in future studies.

Since 2019, the fifth-generation (5G) wireless network has been implemented. Two different frequency ranges available for 5G wireless technology include- frequency range 1 (FR1) and frequency range 2 (FR2). At present, the popular commercial frequency at FR1 was around 2.4 and 3.5 GHz, close to the current 3G and 4G frequencies. The emission power of 5G mobile phones is comparable to that of 3G and 4G terminals. Most of the existed literature, as well as our studies, narrated similar activated sites (frontal and temporal lobules) for different frequencies/modulations. It is, therefore, reasonable to expect that the exposure to new generation wireless signals would result in a similar effect.

The present work also has several limitations. Firstly, our study involved only 34 participants, with 17 under real LTE-EMF exposure. We did not utilize a cross-over experimental design, i.e., the subjects alternatively exposed to real and sham exposure because it may require a washout period. At present, the lasting effect of EMF exposure has been determined. To avoid the ambiguity of this issue, we have decided to use the present experimental design. Secondly, although none of the subjects reported falling asleep, completely ruling out the possibility that subjects fell asleep or experienced sleepiness during the MRI scan was difficult. To eliminate the possibility of falling asleep, we will employ MRI-compatible physiological monitors in future studies. Thirdly, an in-depth understanding of the exposure effect can be achieved by varying the exposure time durations. We did not conduct experiments with various durations, and we have planned to continue the study upon the permission of the ethics committee.

Conclusion

Human brain modulation following LTE exposure was firstly evaluated by functional and network metrics. The topological changes have been reported, and their consistency with the

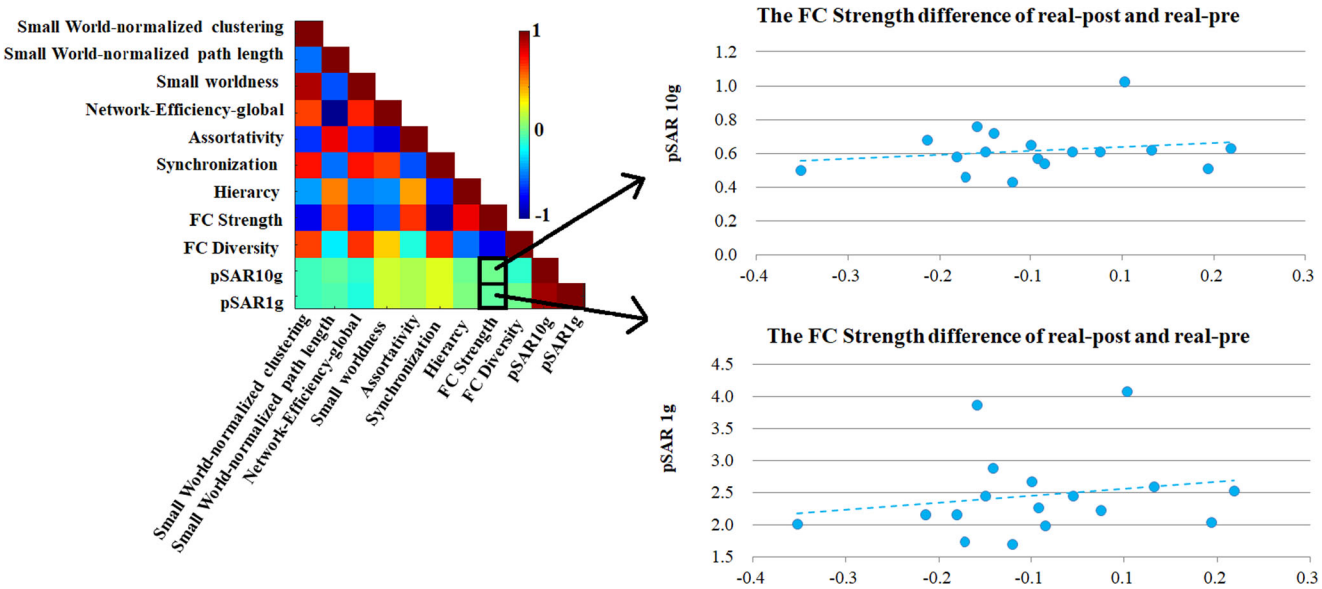

Fig. 8 Correlation matrix of the dosimetric values and the functional and topological metrics

previous analysis was highlighted. Integrating the results from the regional BOLD variation, intraregional similarity, and hypothesis-driven FC analysis, a comprehensive view for the brain activity by the exposure of LTE signal and the signal of next-generation can be obtained. Another novelty was that no correlation was found between the peak SAR values and the altered topological parameters. It demonstrated peak SAR averaged over a certain mass, which was used for assessing the thermal effect of human exposure, was incongruous to quantify the neurophysiological effect of EMF exposure. It may clarify the inconsistency in current human exposure studies.

Availability of data and materials The datasets generated and analyzed during the current study are not publicly available due (data involves the subject's privacy) but are available from the corresponding author on reasonable request.

Authors' contributions Lei Yang and Tongning Wu conceived and designed the study; Lei Yang performed the experiments; Tongning Wu wrote the paper; Chen Zhang reviewed and edited the manuscript; Congsheng Li and Zhiye Chen collection of the data; all authors read and approved the manuscript.

Funding This work was supported by grants from National Natural Science Foundation Project (Grant No. 61971445)

Compliance with ethical standards

Competing interests The authors declare that they have no conflict of interest.

Consent to participate The participants signed consent after the experimental procedure had been fully explained.

Consent to publish The subjects signed informed consent regarding publishing their data, and manuscript is approved by all authors for publication.

References

Aalto S, Haarala C, Bruck A, Sipila H, Hamalainen H, Rinne JO (2006) Mobile phone affects cerebral blood flow in humans. J Cerebr Blood F Met 26:885–890. https://doi.org/10.1038/sj.jcbfm.9600279

Aguirre GK, Detre JA, Alsop DC, D'Esposito M (1996) The parahippocampus Ssubserves topographical learning in man. Cereb Cortex 6(6):823–829. https://doi.org/10.1093/cercor/6.6.823

Bassett S, Bullmore E, Verchinski BA, Mattay VS, Weinberger DR, Meyer-Lindenberg A (2008) Hierarchical organization of human cortical networks in health and schizophrenia. J Neurosci 28: 9239–9248. https://doi.org/10.1523/JNEUROSCI.1929-08.2008

Beggs JM, Plenz D (2003) Neuronal avalanches in neocortical circuits. J Neurosci 23(35):11167–11177. https://doi.org/10.1523/JNEUROSCI.23-35-11167.2003

Burek M, Follmann R, Rosa E (2019) Temperature effects on neuronal firing rates and tonic-to-bursting transitions. Biosystems. 180:1–6. https://doi.org/10.1016/j.biosystems.2019.03.003

C95.1-2019 - IEEE standard for safety levels with respect to human exposure to electric, magnetic, and electromagnetic fields, 0 Hz to 300 GHz. 2019. SASB/SCC39 - SCC39 - International Committee on Electromagnetic Safety , pp.1-312

Catherine W, Patrick W, Virginia P, Robert Z, Todd P, Daniel A, Nina K (2009) Relating structure to function: Heschl's gyrus and acoustic processing. J Hist Neurosci 29(1):61–69. https://doi.org/10.1523/JNEUROSCI.3489-08.2009

Croft R, Leung S, McKenzie R, Loughran S, Iskra S, Hamblin DL, Cooper NR (2010) Effects of 2G and 3G mobile phones on human alpha rhythms: resting EEG in adolescents, young adults, and the elderly. Bioelectromagnetics 31:434–444. https://doi.org/10.1002/bem.20583

Curcio G, Nardo D, Perrucci MG, Pasqualetti P, Chen TL, Del Gratta C, Romani G, Rossini PM (2012) Effects of mobile phone signals over BOLD response while performing a cognitive task. Clin Neurophysiol 123:129–136. https://doi.org/10.1016/j.clinph.2011.06.007

Engel SA, Glover GH, Wandell BA (1997) Retinotopic organization in human visual cortex and the spatial precision of functional MRI. Cereb Cortex 7:181–192. https://doi.org/10.1093/cercor/7.2.181

Haarala C, Aalto S, Hautzel H, Julkunen L, Rinne J, Laine M, Krause B, Hamalainen H (2003) Effects of a 902 MHz mobile phone on cerebral blood flow in humans: a PET study. Neuroreport 14:2019–2023. https://doi.org/10.1097/01.wnr.0000090954.15465.94

Hamblin DL, Croft RJ, Wood AW, Stough C, Spong J (2006) The sensitivity of human event-related potentials and reaction time to mobile phone emitted electromagnetic fields. Bioelectromagnetics 27: 265–273. https://doi.org/10.1002/bem.20209

Hövel P, Viol A, Loske P, Merfort L, Vuksanović V (2018) Synchronization in functional networks of the human brain. J Nonlinear Sci. https://doi.org/10.1007/s00332-018-9505-7

International Commission on Non-Ionizing Radiation Protection (2020) Guidelines for limiting exposure to electromagnetic fields (100 kHz to 300 GHz). Health Physics 118:483–524

Kaiser M, Hilgetag CC (2006) Nonoptimal component placement, but short processing paths, due to long-distance projections in neural systems. Plos Comput Biol 2(7):805–816. https://doi.org/10.1371/journal.pcbi.0020095

Li CS, Wu TN (2015) Dosimetry of infant exposure to power-frequency magnetic fields: Variation of 99th percentile induced electric field value by posture and skin-to-skin contact. Bioelectromagnetics 36(3):204–218. https://doi.org/10.1002/bem.21899

Li CS, Chen Z, Yang L, Lv B, Liu J, Varsier N, Hadjem A, Wiart J, Xie Y, Ma L, Wu T (2015) Generation of infant anatomical models for evaluating electromagnetic field exposures. Bioelectromagnetics 36: 10–26. https://doi.org/10.1002/bem.21868

Lustenberger C, Murbach M, Durr R, Schmid MR, Kuster N, Achermann P, Huber R (2013) Stimulation of the brain with radiofrequency electromagnetic field pulses affects sleepdependent performance improvement. Brain Stimul 6:805–811. https://doi.org/10.1016/j.brs.2013.01.017

Lv B, Chen ZY, Wu TN, Shao Q, Yan Y, Ma L, Lu K, Xie Y (2014a) The alteration of spontaneous low frequency oscillations caused by acute electromagnetic fields exposure. Clin Neurophysiol 125:277–286. https://doi.org/10.1016/j.clinph.2013.07.018

Lv B, Su C, Yang L, Xie Yi, Wu TN (2014b) Whole brain EEG synchronization likelihood modulated by long term evolution electromagnetic fields exposure. 2014 36th Annual International Conference of the IEEE Engineering in Medicine and Biology Society. https://doi.org/10.1109/embc.2014.6943758

Maguire EA, Frackowiak RSJ, Frith CD (1996) Learning to find your way: a role for the human hippocampal region. Philos T R Soc B 263:1745–1750. https://doi.org/10.1098/rspb.1996.0255

McCarty DE, Carrubba S, Chesson AL, Jr Frilot C, Gonzalez-Toledo E, Marino AA (2011) Electromagnetic hypersensitivity: evidence for a novel neurological syndrome. Int J Neurosci 121:670–676. https://doi.org/10.3109/00207454.2011.608139

Menon V, Uddin LQ (2010) Saliency, switching, attention and control: a network model of insula function. Brain Struct Funct 214(5-6):655–667. https://doi.org/10.1007/s00429-010-0262-0

Nakatani-Enomoto S, Yamazaki M, Nishiura K, Enomoto H, Ugawa Y (2020) Effects of electromagnetic fields from long-term evolution on awake electroencephalogram in healthy humans. J Neurosci Res 156:102–107. https://doi.org/10.1016/j.neures.2020.01.010

Penny W, Friston K, Ashburner J, Kiebel S, Nichols T (2011) Statistical parametric mapping: the analysis of functional brain images. Elsevier, Amsterdam

Price CJ (2012) A review and synthesis of the first 20 years of PET and fMRI studies of heard speech, spoken language and reading. NeuroImage 62(2):816–847. https://doi.org/10.1016/j.neuroimage.2012.04.062

Repacholi MH (1999) WHO's international EMF project. Radiation protection dosimetry. Radiat Prot Dosim 83(1-2):1–4. https://doi.org/10.1093/oxfordjournals.rpd.a032642

Robertson JA, Theberge J, Weller J, Drost DJ, Prato FS, Thomas AW (2009) Low-frequency pulsed electromagnetic field exposure can alter neuroprocessing in humans. J R Soc Interface 7(44):467–473. https://doi.org/10.1098/rsif.2009.0205

Roggeveen S, van Os J, Lousberg R (2015a) Does the brain detect 3G mobile phone radiation peaks? An explorative in-depth analysis of an experimental study. PLoS ONE 10(5):e0125390 org/10.1371/journal.pone.0125390

Roggeveen S, van Os J, Viechtbauer W, Lousberg R (2015b) EEG changes due to experimentally induced 3G mobile phone radiation. PLoS ONE 10(6):e0129496. https://doi.org/10.1371/journal.pone.0129496

Rowland JA, Stapleton-Kotloski JR, Dobbins DL, Rogers E, Godwin DW, Taber KH (2018) Increased small-world network topology following deployment-acquired traumatic brain injury associated with the development of post-traumatic stress disorder. Brain Connect 8(4):205–211. https://doi.org/10.1089/brain.2017.0556

Rubinov M, Sporns O (2010) Complex network measures of brain connectivity: uses and interpretations. Neuroimage 52:1059–1069. https://doi.org/10.1016/j.neuroimage.2009.10.003

Simard D, Nadeau L, Kroger H (2005) Fastest learning in small-world neural networks. Phys Lett A 336(1):8–15. https://doi.org/10.1016/j.physleta.2004.12.078

Squire L, Zola-Morgan S (1991) The medial temporal lobe memory system. Science 253:1380–1386. https://doi.org/10.1126/science.1896849

Tombini M, Pellegrino G, Pasqualetti P, Assenza G, Benvenga A, Fabrizio E, Rossini PM (2013) Mobile phone emissions modulate brain excitability in patients with focal epilepsy. Brain Stimul 6:448–454. https://doi.org/10.1016/j.brs.2012.07.006

Tzourio-Mazoyera N, Landeaub B, Papathanassioua D, Crivelloa F, Etarda O, Delcroixa N, Mazoyerc B, Joliota M (2002) Automated anatomical labeling of activations in SPM using a macroscopic anatomical parcellation of the MNI MRI single-subject brain. NeuroImage 15(1):273–289. https://doi.org/10.1006/nimg.2001.0978

Vecchio F, Babiloni C, Ferreri F, Curcio G, Fini R, Del Percio C, Rossini PM (2007) Mobile phone emission modulates interhemispheric functional coupling of EEG alpha rhythms. J Neurosci 25:1908–1913. https://doi.org/10.1111/j.1460-9568.2007.05405.x

Vecchio F, Tombini M, Buffo P, Assenza G, Pellegrino G, Benvenga A, Babiloni C, Rossini PM (2012) Mobile phone emission increases inter-hemispheric functional coupling of electroencephalographic alpha rhythms in epileptic patients. Int J Psychophysiol 84:164–171. https://doi.org/10.1016/j.ijpsycho.2012.02.002

Volkow ND, Tomasi D, Wang GJ, Vaska P, Fowler JS, Telang F, Alexoff D, Logan J, Wong C (2011) Effects of cell phone radiofrequency signal exposure on brain glucose metabolism. JAMA. 305:808–813. https://doi.org/10.1001/jama.2011.186

Wang JH, Zuo XN, Gohel S, Milham MP, Biswal BB, He Y (2011) Graph heoretical analysis of functional brain networks: test-retest evaluation on short-and long-term resting-state functional MRI data. PLoS One 6:e21976. https://doi.org/10.1371/journal.pone.0021976

Wang J, Wang X, Xia M, Liao X, Evans A, He Y (2015) GRETNA: a graph theoretical network analysis toolbox for imaging connectomics. Front Hum Neurosci 9(386):1–16. https://doi.org/10.3389/fnhum.2015.00386

Watts DJ, Strogatz SH (1998) Collective dynamics of' small-world networks. Nature 393:440–442. https://doi.org/10.1038/30918

Wei YW, Yang JY, Chen ZY, Wu TN, Lv B (2019) Modulation of resting-state brain functional connectivity by exposure to acute fourth-generation long-term evolution electromagnetic field: an fMRI Study. Bioelectromagnetics 40:42–51. https://doi.org/10.1002/bem.22165

Wu TN, Lv B, Chen ZY (2012) Dosimetric studies involving in the experiments for the evaluation of the brain activation by LTE exposure. In: Proceedings of international symposium on electromagnetic compatibility (EMC EUROPE), Rome, Italy: IEEE. IEEEXplore. https://doi.org/10.1109/EMCEurope.2012.6396795

Wu T, Shao Q, Yang L (2013) Simplified segmented human models for whole body and localised SAR evaluation of 20 MHz to 6 GHz electromagnetic field exposures. Radiat Prot Dosim 153(3):266–272. https://doi.org/10.1093/rpd/ncs105

Yan CG, Zang YF (2010) DPARSF: a MATLAB tool box for "pipeline" data analysis of resting state fMRI. Front Syst Neurosci 4(13):1–7. https://doi.org/10.3389/fnsys.2010.00013

Yang L, Chen QH, Lv B, Wu TN (2016) Long-term evolution electromagnetic fields exposure modulates the resting state EEG on alpha and beta bands. Clin Eeg Neurosci 48:168–175. https://doi.org/10.1177/1550059416644887

Zang YF, Jiang TZ, Lu YL, He Y, Tian L (2004) Regional homogeneity approach to fMRI data analysis. Neuroimage 22:394–400. https://doi.org/10.1016/j.neuroimage.2003.12.030

Zang YF, He Y, Zhu CZ, Cao QJ, Sui MQ, Liang M, Tian LX, Jiang TZ, Wang YF (2007) Altered baseline brain activity in children with ADHD revealed by resting-state functional MRI. Brain Dev Jpn 29:83–91. https://doi.org/10.1016/j.braindev.2006.07.002

Zhang J, Sumich A, Wang GY (2017) Acute effects of radiofrequency electromagnetic field emitted by mobile phone on brain function. Bioelectromagnetics 38(5):329–338. https://doi.org/10.1002/bem.bioelectromagnetics

Zubko O, Gould RL, Gay HC, Cox HJ, Coulson MC, Howard RJ (2017) Effects of electromagnetic fields emitted by GSM phones on working memory: a meta-analysis. Int J Geriatr Psych. 32:125–135. https://doi.org/10.1002/gps.4581

Publisher's note Springer Nature remains neutral with regard to jurisdictional claims in published maps and institutional affiliations.